Article

Energy-managed soliton fiber laser

Mostafa I. Mohamed [1,2] ✉, **Aurélien Coillet** [1] **& Philippe Grelu** [1] ✉

Ultrafast fiber lasers constitute a flexible platform to investigate new solitary wave concepts. To surpass the low energy limitation of the conventional solitons generated in standard telecom fibers, successive breakthroughs have promoted the usage of an important frequency chirping within fiber oscillators. This lead to original solitary wave regimes such as stretched-pulse, all-normal-dispersion, and self-similar dynamics. We here revisit ultrafast fiber lasers built from standard optical fibers featuring solely anomalous dispersion. We propose a new cavity design enhancing key dissipative effects with contained frequency chirping and demonstrate the generation of high energy pulses in the few-picoseconds regime. The involved intracavity dynamics blends conventional and dissipative soliton features in an unseen way with low- and high-energy propagation regions, allowing an increased flexibility and novel scalability prospects.

The modern era of ultrafast fiber lasers started in the early 90s' when, prompted by the optical communication revolution that spread the internet usage worldwide, reliable single-mode optical fibers and diode laser pumping were becoming widely available. Since then, the cost-effective and energy efficient fiber laser technology has been expanding without pause, replacing countless bulk laser systems in industries and research institutes alike, as well as fostering novel applications in material processing, biotechnology, medicine, defense, and optical metrology[1-4]. In parallel, owing to its accessibility and versatility, the fiber laser platform has developed a special relationship with the fundamental science of laser dynamics and optical solitons, with fruitful comings and goings between experimentation and theory[5,6].

A fundamental soliton is a pulsed waveform that propagates without distortion through balanced interactions with the propagation medium. In a passive optical fiber, a bright soliton can be obtained through a compensation between the Kerr nonlinearity and the anomalous chromatic dispersion which, for standard telecom silica fibers, takes place for optical wavelengths in the low-loss window around 1.5 micron[7,8]. By operating in the anomalous dispersion regime, fiber lasers can therefore generate optical solitons[9]. The fundamental soliton represents an ideal optical pulse, with a bell-shaped chirp-free waveform (i.e. Fourier-transform limited). Nevertheless, it was soon realized that standard optical fibers would only support low energy solitons (in the tens of pJ for a ~1 ps pulse), potentially hampering the outreach and generalization of ultrafast fiber lasers.

Besides, a mode-locked fiber laser is not just a passive fiber link, as it includes nonlinear loss from a saturable absorber mechanism, and gain from a fiber amplifier section. Therefore, the ultrafast laser constitutes a complex nonlinear dissipative system, endowed with a large space of parameters. The wide range of solitary waves that can be generated from fiber lasers has been encompassed into the concept of dissipative solitons, which are localized formations of the electromagnetic field balanced through an energy exchange with the environment in presence of nonlinearity, dispersion and/or diffraction[10]. The research on dissipative optical solitons has been accelerating during the past two decades, following the fundamental discovery of original pulse waveforms and their dynamics[11]. Unlike conventional bright solitons that are exclusively supported by an anomalously dispersive propagation medium, dissipative solitons can form in the normal dispersion regime, where they are found to carry a much higher energy. As a signature of the latter situation, the energy exchange and redistribution within the optical pulse leaves a significant amount of frequency chirping. In fact, the generation of chirped pulses within the fiber laser oscillator has constituted a recurring strategy to find pulse waveforms carrying higher energy, bearing analogy with the chirped-pulse amplification technology developed for optical amplifiers in the mid-80's[12]. Within the fiber laser plaform, such strategy was initiated with dispersion management[13,14] and diversified, successively, in the form of self-similar, all-normal, and giant-chirp ultrafast fiber lasers[15-19], opening the door to multi-nJ ultrashort pulse generation from off-the-shelf fiber technology. More

[1]Laboratoire Interdisciplinaire Carnot de Bourgogne UMR 6303 CNRS, Université de Bourgogne, F-21000 Dijon, France. [2]Department of Physics, Faculty of Science, Alexandria University, Moharram Bek 21511 Alexandria, Egypt. ✉e-mail: mostafa.mohamed@u-bourgogne.fr; philippe.grelu@u-bourgogne.fr

involved intracavity dynamics were introduced in the so-called soliton-similariton fiber laser[20]. The architecture of the latter promoted the propagation of a self-similar highly chirped pulse in a normally-dispersive gain fiber, followed, after spectral filtering, by a low energy soliton propagation in an anomalous passive fiber. Nevertheless, resorting to highly-chirped pulses requires an extra-cavity compression system, and the resulting spectral and temporal waveforms are generally not the desired smooth bell shapes. Can we get the best of both soliton worlds, namely, the energetic (multi-nJ) ultrashort pulses enabled by dissipative soliton dynamics, along with the neat waveforms and moderate frequency chirping that are characteristic of the conventional fiber solitons?

In the present work, we answer positively to the above question by further leveraging the degrees of freedom of the cavity architecture. We emphasize on energy management to delineate high and low energy soliton propagation regions separated by strong nonlinear losses and spectral filtering. In a striking difference with the soliton-similariton laser, we here restrict to the usage of all-anomalous standard fiber components, which constitutes a paradoxical approach to achieve high-energy pulse output from a single fiber laser oscillator. We highlight the blend of conventional and dissipative soliton dynamics inside the cavity, which enables the generation of high-energy bell-shaped pulses with limited frequency chirping. We also demonstrate the unprecedented flexibility of the laser output features and the generation of more complex pulse structures at higher pump power, involving the buildup of higher-order solitons and higher-order soliton molecules.

Results

Generation of multi-nJ single laser pulses

The concept of strong energy management, which is applied to the propagation within all-anomalous optical fibers, is portrayed in Fig. 1a. In most of the cavity, the pulse propagates at low energy and takes the form of a fundamental stationary soliton. This way, the low energy section can include an arbitrary length of passive fiber, within some practical limits. Next, the amplification of the soliton occurs within an optimized length of highly-doped fiber, entailing the pulse energy increase by typically two orders of magnitude, whereas the pulse spectral and temporal broadening remain limited. At the end of the amplification section, above 90% of the pulse energy is output. The pulse remaining in the cavity is spectrally filtered, ensuring the injection of a clean-shaped pulse into the passive fiber that promotes the propagation of a fundamental soliton. Energy management allows containing the frequency chirp accumulated by the pulse, which takes place in the final part of the amplification process owing to self-phase modulation. As a result, a peak power exceeding one kilowatt can be obtained, whatever the pulse duration. Therefore, as a stark contrast with the energy limitation of a conventional ($N = 1$) soliton, whose energy is inversely proportional to the pulse duration, our energy-managed soliton laser delivers output pulses whose energy scales linearly with the pulse duration, as sketched in Fig. 1b.

We have implemented the above energy management concept within the fiber ring laser architecture sketched in Fig. 1c. The gain medium is an erbium-doped fiber (EDF), which amplifies light in the 1535-1590 nm telecom band and features an anomalous chromatic dispersion, with a core size practically the same as that of the single-mode fiber (SMF) that constitutes the remaining sections of the fiber cavity. The laser is mode locked through a virtual saturable absorber effect arising from the nonlinear polarization evolution (NPE) that takes place during pulse propagation in the optical fibers, which is subsequently discriminated by a polarizing beam splitter (PBS). At the end of the amplification stage, the laser field is decoupled from the EDF to propagate in a short free-space section that includes the PBS. One of the two orthogonal polarization components is reflected by the PBS, defining the main output port of the laser[14,21]. In our case, such output

port extracts above 90 % of the intracavity power in the form of high quality energetic pulses, as further developed below. It is followed by an optical isolator for unidirectional laser propagation. Four retarding wave plates allow adjusting the nonlinear transfer function of the virtual saturable absorber to select a stable mode-locked laser regime. To realize the adjustable spectral filter function, we use the combination of a diffraction grating, which disperses spatially the incoming spectral pulse components, with the coupling of the beam into the passive optical fiber (SMF) that continues the laser cavity. The subsequent propagation in the passive SMF fiber takes place at a reduced optical peak power that is comparable to the conventional fundamental ($N = 1$) soliton power. Therefore, the laser architecture allows a great flexibility with respect to the length of SMF used. For instance, we verified that an SMF length ranging from 3 to 100 meters enables to adjust the fundamental cavity repetition rate from ~ 2 – 35 MHz, without affecting much of the pulse features, as discussed further down. For a complementary monitoring and analysis of the laser dynamics, we use a secondary, low power, output coupler that extracts 10 % of the laser power by the end of the passive SMF part of the cavity.

By setting the orientations of the wave plates and the grating, reproducible self-starting mode locking regimes are obtained. The main output port delivers picosecond pulses with typically 1–10 kW of peak power, which are characterized with a free-space frequency-resolved optical gating (FROG) device, a separate second-order autocorrelator, an optical spectrum analyzer, a fast photodetector either connected to an oscilloscope or to a radio-frequency spectrum analyzer, and a dispersive Fourier transform (DFT) measurement setup (see Methods) to visualize the evolution of the laser state roundtrip after roundtrip. Figure 2 displays the features of a typical mode-locked pulse with a FWHM duration of 2.2 ps obtained at a pump power of 1.34 W. The high-energy (PBS) output port yields an average power of 105 mW, which corresponds to a pulse energy E_{PBS} ~3 nJ at the fundamental 34.9 MHz repetition rate. Such pulse energy is about two orders of magnitude higher than the conventional soliton energy ~ 30 pJ that would be supported by the standard anomalous optical fibers used in the cavity, assuming the same pulse duration. This remarkable feature results from the overall highly dissipative cavity design, which incorporates large nonlinear losses, significant spectral filtering, and high gain. Precisely, the applied spectral filtering is crucial to reshape the pulse, allowing the subsequent amplification stage to take place at high gain without being readily affected from the multi-pulsing instability that is otherwise ubiquitous in ultrafast lasers composed of anomalously-dispersive fibers[22]. Another enabling key is that the propagation of high-energy pulses in the fiber waveguide is limited to a short length by the end of the amplifier section, which curtails the accumulated nonlinear phase. As a matter of fact, Fig. 2d displays a bell-shaped spectral pulse profile devoid of any radiation peak—such as the Gordon-Kelly sidebands that plague most of the spectra of anomalous fiber lasers[23,24]. A complete amplitude and phase retrieval of the stable pulse envelope by FROG highlights a gently flat-topped temporal pulse shape with a concave phase profile, as shown in Fig. 2a. The presence of a moderate positive chirp in spite of the anomalous propagation reflects the predominant influence of the self-phase modulation (SPM) on the pulse within the amplifier section. This enables for instance pulse compression by propagation in an anomalous extra-cavity SMF segment, as shown in the Supplementary Discussion, subsection Linear and nonlinear pulse compression.

The present all-anomalous laser cavity supports dissipative solitons of an original nature. It removes the compelling use of normally-dispersive fibers to reach multi-nJ pulse energies in telecom band lasers employing standard fibers, in particular without resorting to the large mode area (LMA) fiber technology. As a matter of fact, the pulse energy achieved here compares well with that obtained in other laser
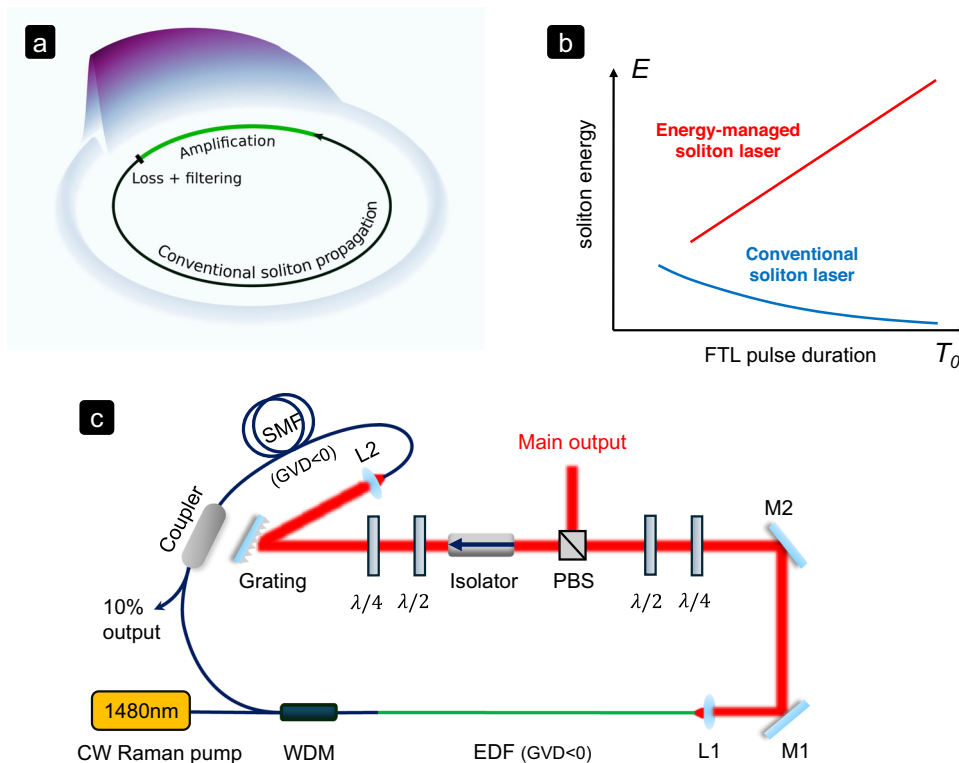
Fig. 1 | Energy-managed soliton fiber laser. a Conceptual figure of an all-anomalous fiber laser cavity featuring strong energy management. The figure sketches the pulse evolution within the cavity roundtrip. **b** Energy (E) versus Fourier-transform limited (FTL) pulse duration (T_0) scaling of the energy-managed soliton laser output, whose trend is opposed to that of conventional soliton lasers. **c** Experimental realization of an energy-managed soliton fiber laser. EDF erbium-doped fiber, SMF single mode fiber, WDM wavelength-division multiplexer, L1, L2 collimating lenses, M1, M2 mirrors, PBS polarization beam splitter. GVD group-velocity dispersion.
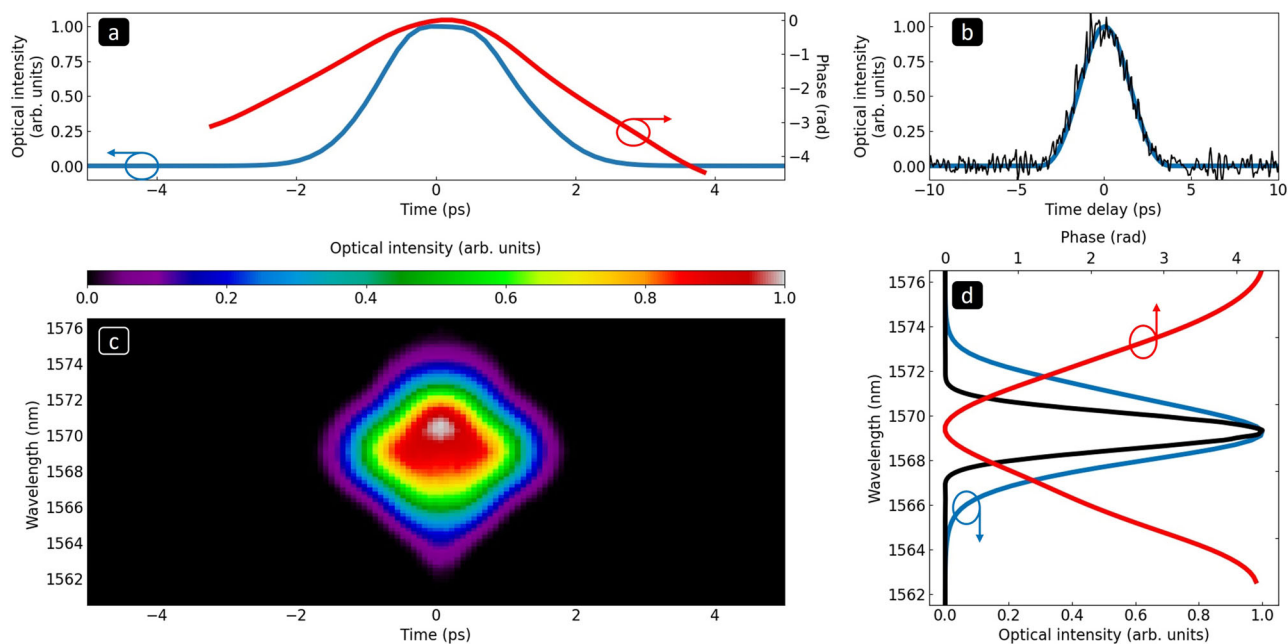

Fig. 2 | Output pulse characterization. The main laser output delivers 3 nJ 2.2 ps pulses at 34.9 MHz, characterized by free-space frequency-resolved optical gating (FROG), which yields: (**a**) The retrieved pulse intensity (blue curve) and phase (red curve); (**b**) the multi-shot second-order auto-correlation trace (blue curve, 3.2 ps at FWMH); (**c**) the FROG spectrogram; (**d**) the pulse optical spectrum (in blue, 3.5 nm at FWHM) and retrieved spectral phase (red curve). For the same laser regime, the secondary output (10% port) delivers 18 pJ pulses, whose second-order multi-shot auto-correlation trace (3.1 ps at FWMH) and optical spectrum (1.75 nm at FWHM) are displayed as black curves for comparison, in (**b**) and (**d**), respectively.

architectures using normally-dispersive fibers, such as dispersion-managed and soliton-similariton cavities[13,17,20]. Nevertheless, in most of the intracavity fiber sections, the pulse propagation takes place at a relatively low power, as monitored from the secondary laser output. The latter displays a 18 pJ pulse energy (0.65 mW average power), a spectral width of 1.75 nm, and a 2 ps pulse duration, see Fig. 2b and d.

To gain a deeper understanding of the laser intracavity dynamics, we conducted numerical simulations of the pulse propagation in the cavity sketched in Fig. 1, using an extended nonlinear Schrödinger equation model for the fibers and discrete transfer functions for lumped optical elements, see the Methods section for details. The simulation results presented in Fig. 3 can be summarized as follows. A low-energy, nearly chirp-free soliton pulse is transferred from the passive SMF to the amplifier fiber section. The amplification procures a large gain of the order of 20 dB, resulting in a high-energy pulse that becomes subjected to spectral broadening and pulse compression as it propagates in the anomalous dispersion fiber, as seen in Fig. 3e,g. The simulation retrieves the positive chirp, which is calculated across the pulse peak, as shown in Fig. 3f. Above 85% of the pulse energy is extracted by virtue of the effective saturable absorber effect. Finally, the pulse is spectrally filtered, which removes most of its chirp and allows soliton-like propagation after being re-coupled into a standard SMF fiber.

The soliton-like propagation within the SMF allows us to alter the length of that SMF section while maintaining the overall dynamical stability, which we first demonstrate numerically (Supplementary Fig. 3). We experimentally confirm this feature, obtaining mode locking with nearly identical pulse outputs after incorporating various SMF fiber lengths, up to 100 meters. In these experiments, we select, through adequate pump power levels, a pulse energy yielding ~1 nJ at the main output, see Fig. 4a. Over widely variable repetition rates, the 1-nJ pulse energy is obtained for nearly identical pulse durations, which also entails operating at a reduced pump power when the repetition frequency is lowered, as shown in Fig. 4b.

In the following, we demonstrate the possibility to output higher pulse energy and average power. We operate at a 34.9 MHz repetition rate and increase the pump power to 1.58 W. The main output port yields an average power of 160 mW, corresponding to a pulse energy, peak power, and duration, of 4.6 nJ, 2 kW, and 2.2 ps, respectively. At such peak power level, the pulse starts featuring significant deformations in both spectral and time domains, as seen from the FROG retrieval displayed in Fig. 5. From simulations, we estimate that most of these deformations take place during the final propagation stretch of ~25 cm within the amplifier section. Since the pulse propagates in the anomalous dispersion regime, these spectral and temporal pulse deformations are associated with the initial stage of the propagation of a higher-order soliton, where spectral broadening and frequency chirping are expected to acquire an important magnitude. This is reflected in the calculated Fourier-transform limited pulse duration, which goes down to around 0.4 ps, a value six times lower than the FWHM pulse duration. Accordingly, a lower estimate of the soliton number is $N \simeq 3.4$. To gain further insight into this higher-order soliton, we test its propagation outside the cavity within different segments of SMF (Supplementary Fig. 8).

Bifurcation toward soliton molecules

Further increase of the pump power—all other laser parameters being fixed—results in a bifurcation toward multi-pulse dynamics. To gain a deeper insight of that transition process, we record optical spectra in real time using the time-stretch DFT technique (see Methods). A typical scenario is represented in Fig. 6, where 3500 consecutive laser output spectra and their Fourier transforms are displayed. We highlight three successive phases of the transition. First, Fig. 6i, iv show the dynamics before the multi-pulse transition: the pulse's spectral and related temporal deformations display a striking similarity with higher-order soliton dynamics. Noting that they take place over consecutive roundtrips and not along a homogeneous propagation medium, they bear a closer relationship with
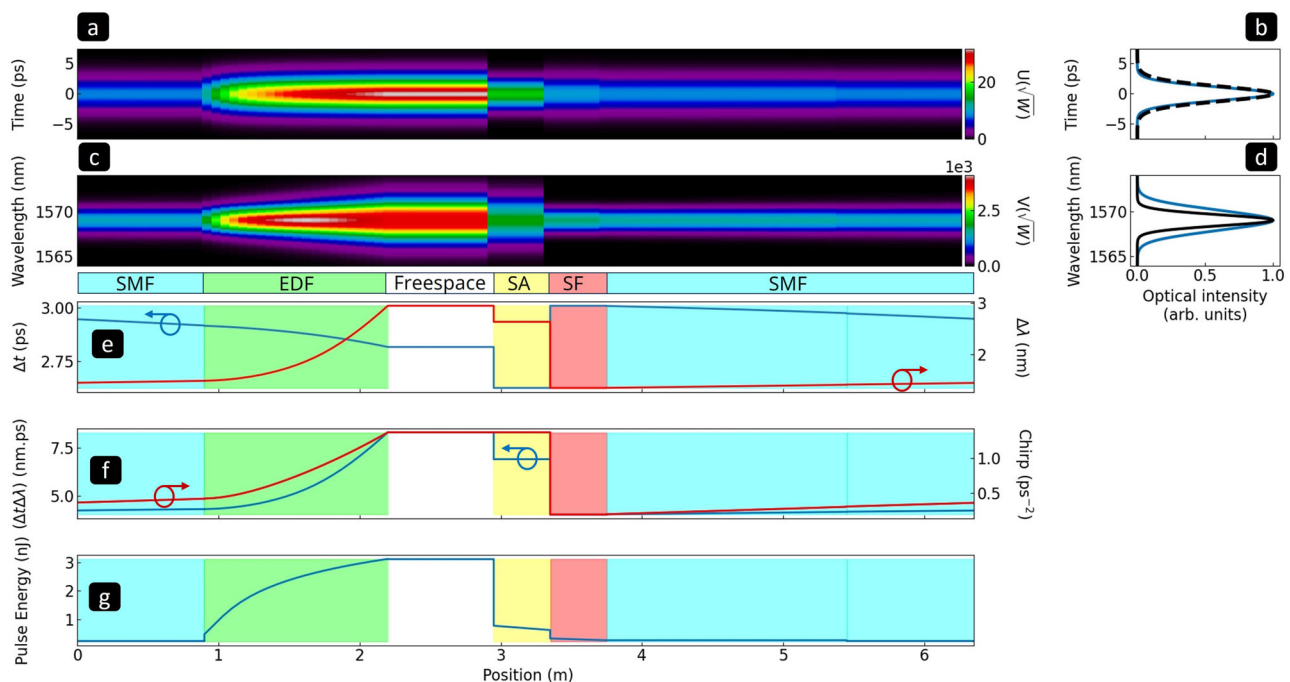

Fig. 3 | Numerical simulation of the intracavity pulse dynamics. Colormaps of the temporal and (**c**) spectral fields evolution within a single cavity roundtrip, obtained in the stationary mode locking regime. Snapshots of (**b**) the temporal intensity and (**d**) spectrum of the main (blue curves) and 10% (black dashed curves) output ports. **e** Evolution of the full width at half maximum (FWHM) pulse width (blue curve) and of the spectral width (FWHM, red curve). SMF passive single-mode fiber, EDF erbium-doped fiber, SA saturable absorber, SF spectral filter. **f** Evolution of the time-bandwidth product (FWHM, blue curve) and the frequency chirp (red curve). **g** Evolution of the pulse energy.
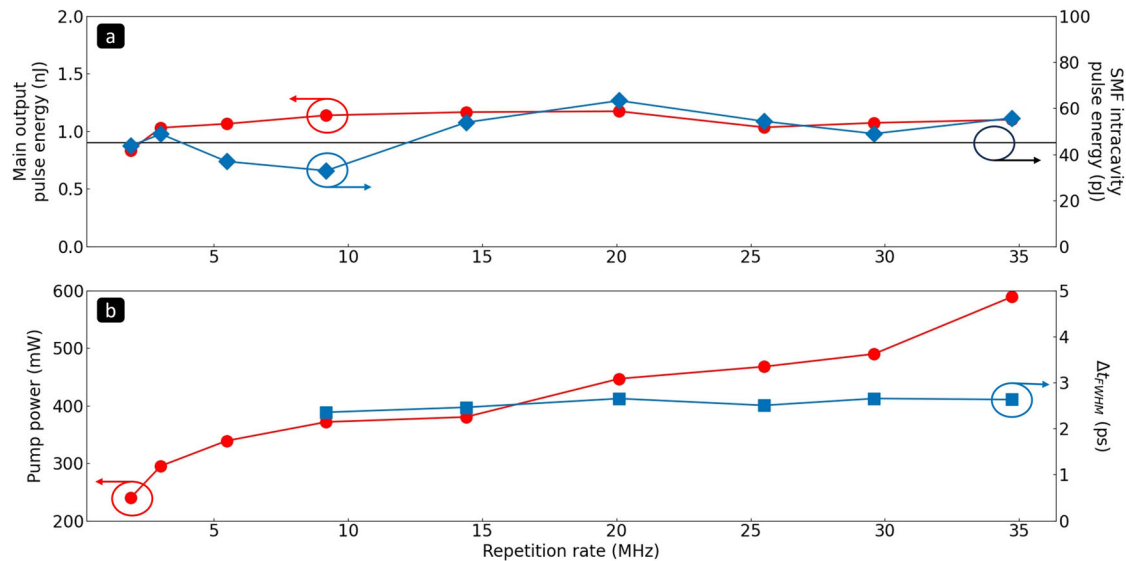
Fig. 4 | Flexible pulse repetition rate in experiments. Single pulse features are obtained by changing the passive single-mode fiber (SMF) length while fixing the output pulse energy close to 1 nJ. **a** The main laser output pulse energy (in red) and the intracavity pulse energy along the SMF section (in blue) compared with the conventional (N = 1) soliton energy (45 pJ for a 1.45 ps FWHM pulse). **b** The corresponding pump power (in red) and pulse duration of the main laser output port (in blue).
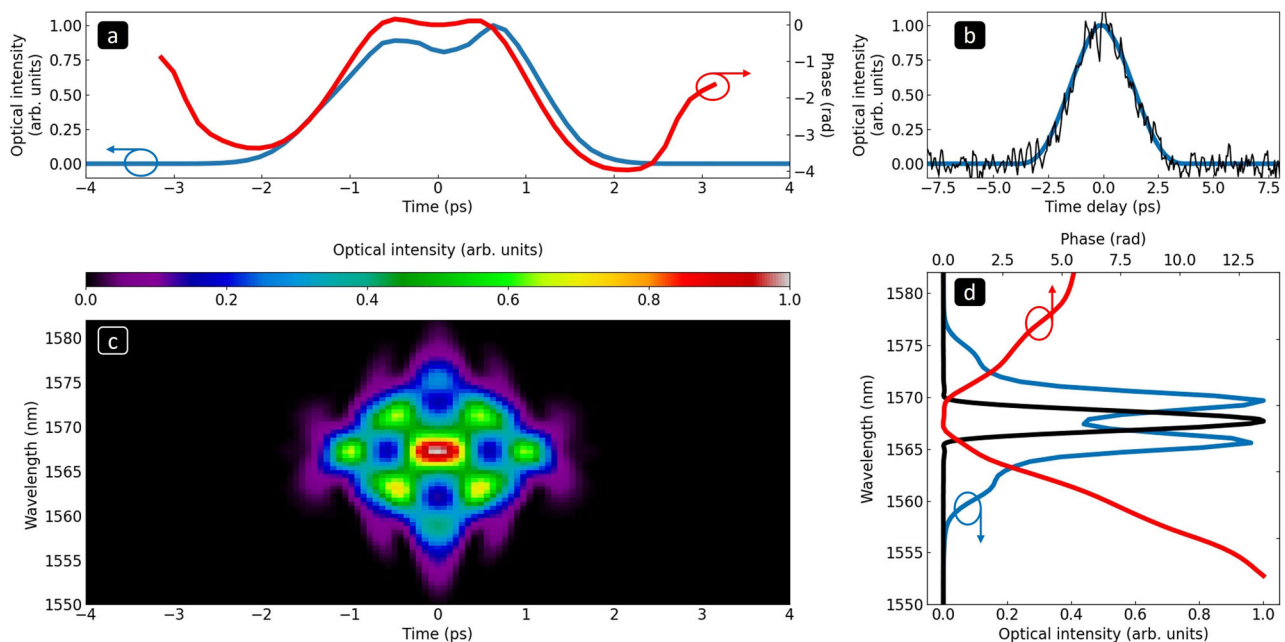

Fig. 5 | Pulse characterization close to the pulse breakup transition. The main laser output delivers 4.6 nJ 2.2 ps pulses at 34.9 MHz, characterized by free-space frequency-resolved optical gating (FROG), which yields: (**a**) The retrieved pulse intensity (blue curve) and phase (in red); (**b**) the second-order auto-correlation trace (blue curve); (**c**) the FROG spectrogram; (**d**) the pulse optical spectrum (in blue) and retrieved spectral phase (red curve). In the same regime, the secondary output (10% port) delivers 16 pJ pulses, whose second-order auto-correlation trace (2.9 ps FWHM) and optical spectrum (2.0 nm FWHM) are displayed as black curves in (**b**) and (**d**).

the pulsating spectral dynamics that have been recently reported in ultrafast lasers[25–28]. Indeed, Fig. 6c,d highlight long-period spectral pulsations around the central wavelength, which are attributed to the excess of SPM[28]. In essence, an excess of SPM within the anomalous propagation regime initiates a high-order soliton propagation, which triggers dissipative soliton pulsations over consecutive cavity roundtrips: we here have an original blend of conventional (higher-order soliton) and dissipative (limit cycle attractor) soliton dynamics.

This initial phase is followed by a second one, depicted in Fig. 6ii,v: pulse breakup occurs and a bound state of two solitons, namely an optical soliton molecule, takes shape over a few cavity roundtrips. We note the absence of dispersive waves in the process, in contrast to what is routinely observed for multi-pulse transitions taking place in anomalous fiber lasers[22,23]. We attribute this feature to the presence of a relatively strong spectral filter, as confirmed by numerical simulations (see Suppl. Fig. 4). Over the subsequent roundtrips, the soliton molecule undergoes a significant spectral
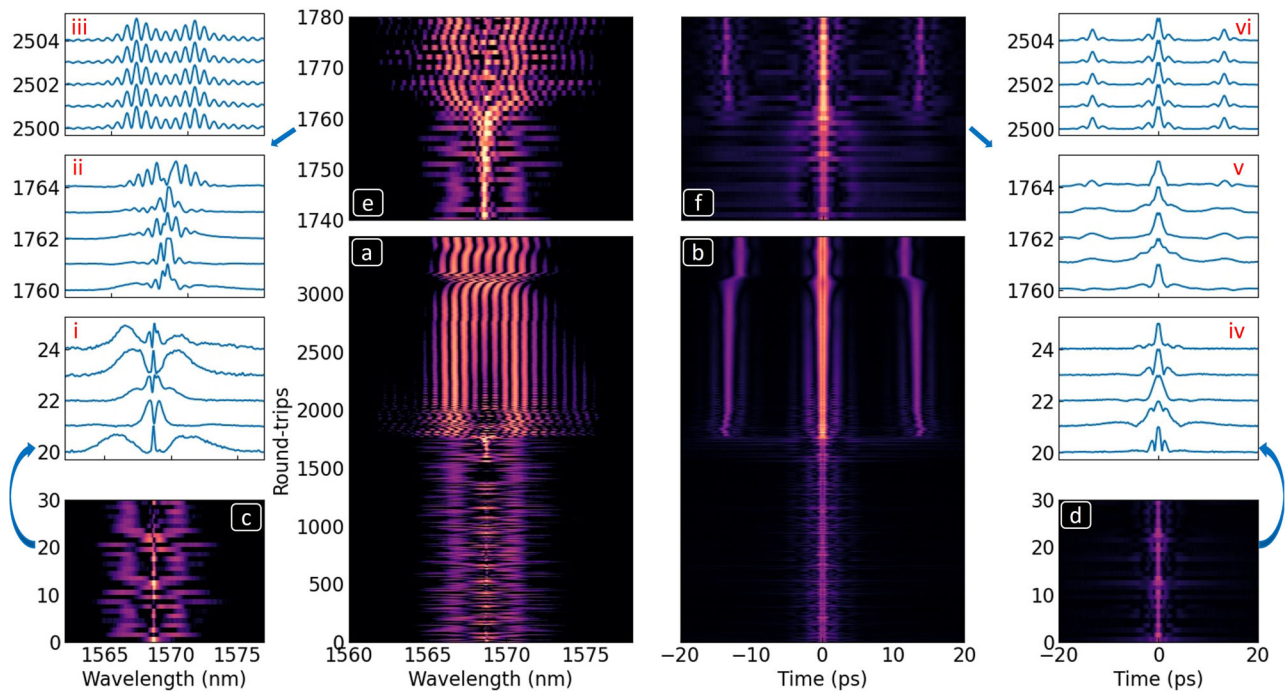
Fig. 6 | Transient dynamics: from pulsating higher-order soliton (HOS) to higher-order soliton molecule (HOSM). a Dispersive Fourier-transform (DFT) recording of single-shot optical spectra over 3500 consecutive roundtrips. **b** Evolution of the Fourier transform of the DFT spectra (first-order temporal autocorrelation traces). **c** Close-up showing the spectral pulsation over 30 roundtrips and (**d**) their Fourier transforms. **e** Close-up of DFT spectra from 1740 to 1780 roundtrips highlighting the transition to HOSM. **f** Evolution of the Fourier transform of the DFT spectra displayed in (**e**). **i,ii,iii** DFT spectra of five successive roundtrips: **i** before, **ii** along, and **iii** after the transition; **iv,v,vi** FFT of the DFT spectra for the same successive roundtrips: **iv** before, **v** along, and **vi** after the transition.

broadening, then acquires a marginal stability from roundtrips ~2000 – ~3000, see Fig. 6. The soliton molecule spectra and their Fourier transforms in Fig. 6iii,vi are signatures of higher-order solitons: remarkably again, the laser dynamics blends typical dissipative soliton dynamics—here, a soliton molecule attractor—with conventional higher-order soliton propagation that takes place within a delineated part of the laser cavity.

In subsequent runs, we adjust the laser parameters to reach a stationary higher-order soliton molecule (HOSM). Figure 7 is an example of a stable HOSM consisting of two bound pulses separated by 6 ps, obtained at a pump power of 1.58 W and a repetition rate of 18.65 MHz. The main output port delivers an average power of 185 mW, corresponding to a 10 nJ HOSM. It is instructive to compare the stationary soliton molecule features observed from the two laser outputs. The optical spectrum taken from the main output, see Fig. 7a, displays a broad modulation that originates from higher-order soliton dynamics, as well as highly-contrasted short-period fringes that indicate the stable self-locking between the two soliton pulses. The secondary output displays spectral fringes of the same periodicity, and the second-order optical autocorrelation (Fig. 7b) measures the corresponding relative separation at 6.0 ps from both output ports. Nevertheless, the soliton molecule is significantly affected by spectral filtering, which shrinks its optical bandwidth by roughly a factor of three. The individual pulse duration is still measured at ~3 ps: this indicates the removal of most of the frequency chirping by the localized spectral filter, leaving a nearly chirp-free low-energy soliton molecule after recoupling into the passive SMF fiber section. The experimental recordings are well reproduced by the numerical simulations of the laser dynamics. In our experiments and numerical simulations alike, stationary soliton molecules were always composed of two identical solitons. The simulated case displayed in Fig. 7c, d corresponds to the stationary soliton molecule obtained after 80 cavity roundtrips in Supplementary Fig. 7 (see also its dynamical

buildup in the Supplementary Movie 1). In spite of being stationary over successive roundtrips, the molecule is drastically affected by the strength of the dissipative effects taking place along a single roundtrip. In the final stretch of the amplifier section, the pulses inherit higher-order solitons traits, forming a higher-order soliton molecule (HOSM). After being subjected to the removal of 90 % of its energy and to spectral filtering, the soliton molecule takes the form of a pair of fundamental NLS solitons, which propagates without significant deformation along a relatively long SMF link, features confirmed by the numerical simulations.

Discussion

Our study has revealed that an intracavity spectral filter provides an additional degree of freedom that can be leveraged to increase and optimize the output pulse energy by more than two orders of magnitude. We find that reducing its bandwidth allows for a higher-energy pulse extraction, following an optical amplification at higher gain. Although our experiments already demonstrate remarkable output energies in the few nJ range, simulations predict the generation of pulse energies in excess of 50 nJ, when the filter bandwidth goes down to 0.2 nm (see Supplementary Fig. 5). These simulations support the conceptual scalability picture displayed in Fig. 1b, where the pulse energy is increased along with the pulse duration, as the filter bandwidth is reduced. In the current experiment, the pulse energy was successfully increased to 12 nJ when the filter bandwidth was reduced to 1 nm, keeping a single pulse per cavity roundtrip. The characterization of this mode locked regime is presented in Supplementary Fig. 6. The pulse features a flat-top intensity profile of 3.4 ps duration, which corresponds to a peak power ~3.5 kW. Investigating the role of the spectral filter further, let us mention the prospect of varying its profile as an additional degree of freedom to pilot the pulse dynamics. Such prospect is introduced in the subsection "Impact of the spectral filter shape" of the Supplementary Discussion.
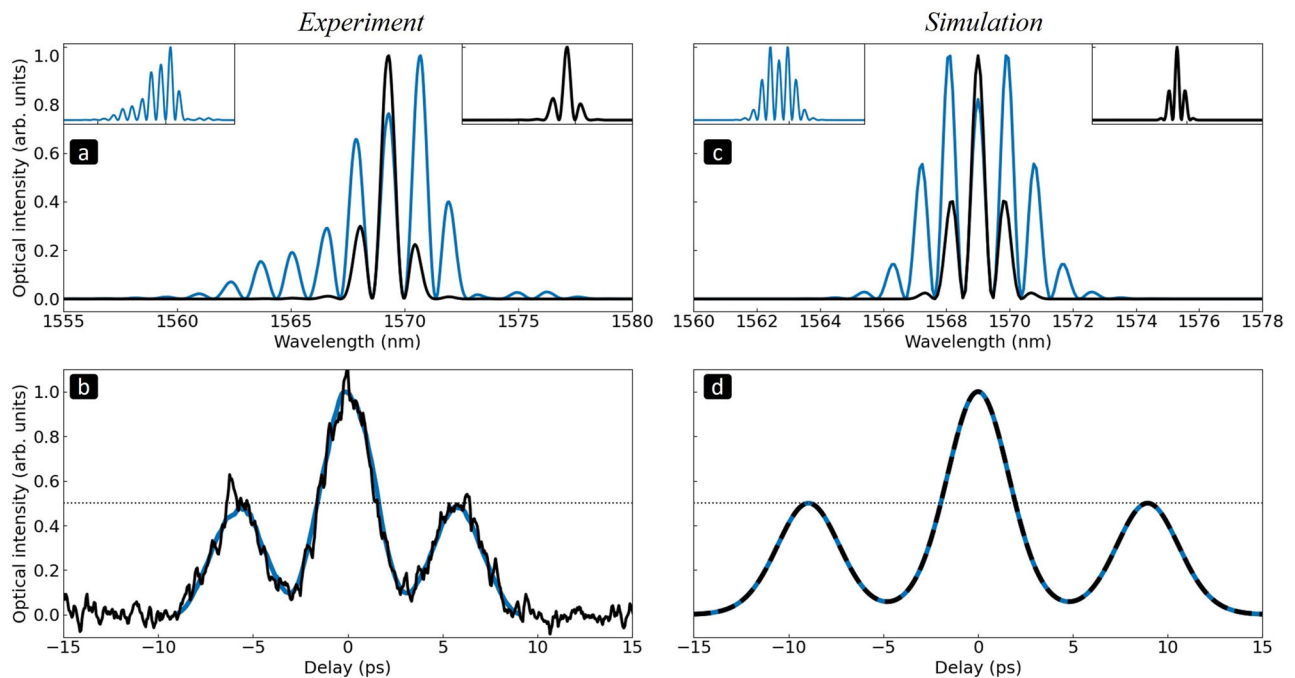
Fig. 7 | Characterization of a 10-nJ stationary soliton molecule. a Optical spectrum recorded from the main output (in blue) and from the secondary 10% port (in black) by the optical spectrum analyzer. **b** Multi-shot second-order autocorrelation recorded from the main output (in blue) by the FROG device compared with the second-order autocorrelation from the 10% port (black curve). **c**, **d** are the spectral and temporal intensity profiles obtained by numerical simulation of the laser dynamics.

Our pulse characterization platform relies on FROG for the retrieval of stationary (stable) output pulse dynamics and on DFT for capturing real time transients. Both provide accurate experimental information that are consistent with numerical simulations. In the prospect of exploring additional complex picosecond dynamics and transients that can be generated from the laser architecture, we note that the characterization could benefit from additional techniques, such as the coherent homodyne detection, yielding a full-field retrieval, as well as its analysis through the nonlinear Fourier transform method[29,30].

A great advantage of the present laser architecture is that it allows delivering nearly identical pulse features (pulse profile, energy, peak power) at various repetition rates, according to the length of the SMF that serves as a compact soliton delay line in the low-energy part of the cavity. We presented above (Fig. 4) an illustration of this feature in a range of repetition rates spanning over more than a decade. Could we extend further such scalability to below MHz repetition rate, therefore reaching exceptional pulse energies at pump powers scaled down below 100 mW? First, the pump source should be changed to reach a stable cw pumping at relatively low power. Beyond such straightforward technical modification, some physical impairments are expected to arise at repetition rates of the order or smaller than 100 kHz. A first set come from the SMF fiber length, which will induce additional propagation losses and possible polarization instability, though the latter issue can be solved by employing a polarization-maintaining fiber. Another set arise from the laser physics, where the amplified spontaneous emission noise and gain relaxation dynamics are expected to degrade the laser performance. Nevertheless, such direction remains an interesting prospect.

Within standard telecom optical fibers, few-ps pulses having a peak power as large as 3.5 kW readily enter a higher-order propagation regime, entailing a significant amount of SPM and associated chirp. If we wish to contain the frequency chirping effect and keep bell-shaped output pulses, simulations show that it is advisable to remain below

2 kW of peak power. Following the latter approach, the subsequent increase of the pulse energy should rely on the corresponding increase of the pulse duration. This outcome is reminiscent of the concept of a dissipative soliton resonance (DSR)[31]. Theoretically, DSR occurs in the close vicinity of a hypersurface in the space of parameters of the equation governing propagation in a dissipative nonlinear medium. Pulsed solutions can therefore acquire virtually unlimited energies as soon as the equation parameters converge toward that specific hypersurface. For laser systems, it means that by tuning one or several cavity parameters, both pulse duration and energy increase by orders of magnitude, whereas the peak power remains clamped[32]. The translation of the DSR concept into laser experiments generating coherent and compressible pulses has not proven to be straightforward[33]. Whereas DSR involves spreading linear and non-linear chirps, the present energy-managed soliton approach opts out pulse stretching. In energy-managed soliton dynamics, the increase of the pulse duration is achieved by reducing the spectral filter bandwidth, therefore containing frequency chirping and keeping bell-shaped temporal intensity profiles.

A possible strategy to further extend the performance of the energy-managed soliton fiber laser concept would be to control the mechanisms allowing higher-order soliton dynamics to unfold further. This would also be reminiscent of the 1984 original soliton laser concept, where the laser cavity included a self-consistent $N = 2$ soliton propagation in a passive SMF link[9]. To date, fiber laser simulations and experiments alike show that the propagation of higher-order solitons over a soliton soliton period within a dissipative fiber laser cavity is not supported, or more precisely, does not lead to a stable attracting state for the laser dynamics[5]. This nevertheless remains a challenging fundamental and practical perspective.

More naturally, the proof of concept provided in this article will find a natural development with the use of specialty fibers, such as LMA fibers[34,35]. With the latter, it should be easy to break into the microjoule pulse energy domain without resorting to the dispersive pulse stretching.

The concept of energy-managed soliton laser is also particularly suitable to the generation of energetic picosecond pulses in the 2-micron wavelength region, owing to the larger anomalous dispersion of silica at such wavelengths, and to the availability of efficient thulium and thulium-holmium optical amplifiers. Besides, whereas the present fiber laser architecture benefits from a free space section to efficiently manipulate the polarization where the optical field has the highest intensity, it should be possible to reach a satisfactory trade off between pulse energy optimization and laser ruggedness, and develop all-fiber energy-managed soliton lasers, as discussed in the last subsection of the Supplementary Discussion.

We also expect a translation of the energy-managed soliton fiber laser concept into the area of spatiotemporal mode locking[36,37], which utilizes multimode optical fibers and has a potential for pulse energy upscaling[38]. To conclude, we anticipate that the present cavity concept, which reveals unprecedented flexibility and scalability of the laser output and is easily translatable into all major fiber laser platforms, will lead to further fundamental exploration as well as outstanding fiber laser development when combined with advanced optical fiber technology.

Methods

Experimental setup

The technical details concerning the fiber laser setup shown in Fig. 1 are as follows. The erbium-doped fiber (EDF, Liekki ER80-8/125) has a high doping level and features anomalous dispersion over the 1535–1590 nm lasing window. At 1550 nm, its mode field diameter and group velocity dispersion are, respectively, 9.5 μm and -25.5 ps^2 km^{-1}. The EDF is pumped at 1480 nm by a Raman fiber laser (KEOPSYS, optical power up to 8 W) coupled through a wavelength-division multiplexer (WDM, Thorlabs WD 1450B). To optimize the length of the erbium-doped fiber (EDF), we first numerically assessed a length range for the amplifying section, from the technical information available. We initially sought an optimal self-compression point arising by the end of the EDF, though such length varied along with the targeted pulse energy and related pump power. We showed a possibility to reach pulse energies in excess of 20 nJ with a 1 meter long EDF. Nevertheless, the current fiber doping led us to increase the EDF length to 1.5 meter to reach a satisfactory pump absorption ratio of 90%, as well as an overall saturated gain in excess of 20 dB, which we validated in a separate experimental testing of the amplifier section. At the end of the amplification stage, the laser field is decoupled from the fiber and collimated by the lens L1. The beam propagates through a 80 cm long free-space section, where its polarization is accurately controlled by quarter- and half-wave retarding plates. Owing to the nonlinear polarization evolution (NPE) taking place during pulse propagation in the optical fibers, the polarization discrimination through the polarizing beam splitter (PBS) enables a virtual saturable absorber effect. The rejection port of the PBS serves as the main laser output port[14,21], which typically extracts above 90 % of the intracavity power. The PBS is followed by a free space, polarization sensitive optical isolator ensuring unidirectional lasing, as well as by retarding waveplates. The whole set of waveplates allows adjusting precisely the nonlinear transfer function of the NPE-based virtual saturable absorber effect. The free space section is continued with a diffraction grating (600 lines/mm) with 85% efficiency from which the (-1) reflected diffraction order is directed onto a passive optical fiber (Corning SMF-28e) after being focused by the lens L2. Together, the diffraction grating and the finite core size and numerical aperture of the SMF make a flexible bandpass spectral filter, whose central wavelength is selected through rotation of the grating. The free-space-to-fiber coupling efficiency, taking into account the diffraction efficiency, is (68 ± 2) % and depends slightly on the central wavelength. The filter bandwidth is adjusted by either changing the grating-to-fiber distance or by inserting an optical telescope between the two. The results presented in this work have been obtained with a bandwidth of either 1.65 nm or 1.0 nm.

The length of the passive fiber is widely adjustable, benefiting from the propagation without significant deformation of a soliton pulse close to the fundamental ($N = 1$) soliton. Such propagation is assessed by a secondary laser output, obtained from the 10% port of an intracavity 90/10 fiber coupler.

The pulses leaving the main laser output are characterized in the spectro-temporal domain with a free-space frequency-resolved optical gating device (Femto Easy Fast FROG PS10). The secondary laser output has an average power that is typically 10^2 to 10^3 times lower than that of the main one. It is monitored with an optical spectrum analyzer (Anritsu MS9710B), as well as with a fast photodetector (OE695G, 9.5 GHz) connected to a 6 GHz oscilloscope (LeCroy WP-760Zi, 40GSa/s). A home-made second-order background-free auto-correlator complements the temporal analysis, having a long scan range of 300 ps that is suitable to verify the absence of multiple pulsing, complementarily to the oscilloscope recordings.

The output pulse spectra are also analyzed in real time, using the time-stretch dispersive Fourier-transform (DFT) technique. It consists in propagating the output pulses linearly in a highly dispersive medium, so that in the far-field dispersion regime, the temporal profile of the stretched pulse maps its optical spectral intensity profile[26,28]. Here, the highly dispersive medium is a 6.3 km long dispersion compensation fiber (DCF), resulting in an accumulated dispersion of 680 ps km^{-1} at the pulse central wavelength. The stretched pulse intensity is then detected using a high-speed photodiode (OE695G, 9.5 GHz) and recorded on the real-time digital oscilloscope (6 GHz). The resulting DFT spectral resolution is 0.3 nm in the C+L optical telecom bands.

Numerical simulations

The simulations are based on a scalar parameter-managed fiber laser model. One intracavity loop retains the following sequence of elements: a short length of passive fiber (SMF) followed by the gain fiber (EDF), a free-space section containing an instantaneous saturable absorber (SA), a bandpass spectral filter (SF), and a flexible length of SMF. Propagation in the EDF follows a generalized nonlinear Schrödinger equation:

$$\frac{\partial U}{\partial z} + i\frac{\beta_2}{2}\frac{\partial^2 U}{\partial t^2} = \frac{g-\alpha}{2}U + i\gamma|U|^2 U + \frac{g}{2\Omega_g^2}\frac{\partial^2 U}{\partial t^2}, \qquad (1)$$

where U, the slowly-varying envelope of the electric field, is a function of both propagation coordinate z and local time t in the reference frame co-moving with the pulse. β_2, g and α are the fiber group velocity dispersion (GVD), differential gain and loss, respectively. γ is the effective third-order nonlinear coefficient and Ω_g represents the EDF gain bandwidth, which corresponds to ~15 nm in the wavelength domain. The differential gain is expressed as:

$$g = g_0 \exp\left(-\frac{E_p}{E_{sat}}\right). \qquad (2)$$

Here, g_0 represents the small signal gain, E_{sat} stands for the gain saturation energy, which is proportional to the pump power, and E_p is the energy of the pulse at location z. Hence, the first and third terms on the right-hand side of Equation (1) account for the dissipative effects resulting from gain saturation and spectral filtering occurring within the doped fiber. The propagation within SMF sections is calculated by setting $g = 0$ and $\alpha = 0$ in Equation (1), which then takes the form of a standard NLS equation. For the sake of simplification, the saturable absorber (SA) is modeled by an instantaneous nonlinear transfer

function, expressed as:

$$T(t) = 1 - \left[q_n + \frac{q_0}{1 + \frac{P(t)}{P_{sat}}} \right] \qquad (3)$$

where q_n is the linear loss, q_0 the saturable modulation depth, $P(t)$ is the instantaneous pulse power, and P_{sat} is the saturation power of the SA.

The above numerical model consistently exhibits qualitative and quantitative agreements with the experimental results. It is solved with a standard split-step Fourier method algorithm, where stable solutions have been reproduced from different initial white noise field conditions. The numerical simulations employ parameters that align with their corresponding experimental values. In the experiments, we have the capability to manipulate the repetition rate (achieved by adjusting the length of the single-mode fiber, SMF), pump power, nonlinear transfer function, and spectral filtering.

The EDF is 1.5 m long, has a mode field diameter (MFD) of 9.5 μm, $\beta_2 = -25.5$ ps^2 km^{-1}, and $\gamma = 1.4$ W^{-1}km^{-1} at a wavelength of 1569 nm. The remaining part of the cavity consists of 3.5 m of SMF, the length of which is subsequently increased to lower the repetition rate and demonstrate the soliton propagation in the low energy section. We use the following SMF values: MFD = 10.4 μm, $\gamma = 1.7$ W^{-1}km^{-1}, and $\beta_2 = -22.8$ ps^2 km^{-1}. For the saturable absorber function, we set $q_n = 0.65$, $q_0 = 0.35$ and $P_{sat} = 100$ W. As for the gain, we specify $E_{sat} = 0.7$ nJ to achieve an intra-cavity pulse energy of ~ 3 nJ. This value corresponds to the measured result for the 35 MHz repetition rate, as illustrated in Fig. 3 and validated by experimental data presented in Fig. 2.

Data availability

The datasets generated in this study have been deposited in the CNRS database under the following accession link: https://src.koda.cnrs.fr/aurelien.coillet.4/energy-managed-soliton-fiber-laser/.

References

1. Richardson, D. J., Nilsson, J. & Clarkson, W. A. High power fiber lasers: current status and future perspectives. *J. Opt. Soc. Am. B* **27**, B63 (2010).
2. Fibre laser focus. *Nat. Photon.* **7**, 841 (2013).
3. Shi, W., Fang, Q., Zhu, X., Norwood, R. A. & Peyghambarian, N. Fiber lasers and their applications. *Appl. Opt.* **53**, 6554 (2014).
4. Kim, J. & Song, Y. Ultralow-noise mode-locked fiber lasers and frequency combs: principles, status, and applications. *Adv. Opt. Photon.* **8**, 465–540 (2016).
5. Grelu, P. Solitary waves in ultrafast fiber lasers: from solitons to dissipative solitons. *Opt. Commun.* **552**, 130035 (2024).
6. Blanco-Redondo, A., de Sterke, C. M., Xu, C., Wabnitz, S. & Turitsyn, S. K. The bright prospects of optical solitons after 50 years. *Nat. Photonics* **17**, 937 (2023).
7. Hasegawa, A. & Tappert, F. Transmission of stationary nonlinear optical pulses in dispersive dielectric fibers. 1—anomalous dispersion. *Appl. Phys. Lett.* **23**, 142 (1973).
8. Mollenauer, L. F., Stolen, R. H. & Gordon, J. P. Experimental observation of picosecond pulse narrowing and solitons in optical fibers. *Phys. Rev. Lett.* **45**, 1095 (1980).
9. Mollenauer, L. F. & Stolen, R. H. The soliton laser. *Opt. Lett.,* **9**, 13–15 (1984).
10. Grelu, P. & Akhmediev, N. Dissipative solitons for mode-locked lasers. *Nat. Photonics* **6**, 84–92 (2012).
11. Ferreira, M. *Dissipative Optical Solitons*. 1st edn, Vol. 364 (Springer Series in Optical Sciences, 2022).
12. Maine, P., Strickland, D., Bado, P., Pessot, M. & Mourou, G. Generation of ultrahigh peak power pulses by chirped pulse amplification. *IEEE J. Quantum Electron.,* **24**, 398–403 (1988).
13. Tamura, K., Ippen, E. P., Haus, H. A. & Nelson, L. F. 77-ps pulse generation from a stretched-pulse mode-locked all fiber ring laser. *Opt. Lett.* **18**, 1080–1082 (1993).
14. Tamura, K., Doerr, C. R., Nelson, L. E., Haus, H. A. & Ippen, E. P. Technique for obtaining high-energy ultrashort pulses from an additive-pulse mode-locked erbium-doped fiber ring laser. *Opt. Lett.* **19**, 46–48 (1994).
15. Fermann, M. E., Kruglov, V. I., Thomsen, B. C., Dudley, J. M. & Harvey, J. D. Self-similar propagation and amplification of parabolic pulses in optical fibers. *Phys. Rev. Lett.* **84**, 6010 (2000).
16. Ilday, F. Ö., Buckley, J. R., Clark, W. G. & Wise, F. W. Self-similar evolution of parabolic pulses in a laser. *Phys. Rev. Lett.* **92**, 213902 (2004).
17. Chong, A., Renninger, W. H. & Wise, F. W. All-normal-dispersion femtosecond fiber laser with pulse energy above 20 nJ. *Opt. Lett.* **32**, 2408–2410 (2007).
18. Kelleher, E. J. R. et al. Generation and direct measurement of giant chirp in a passively mode-locked laser. *Opt. Lett.* **34**, 3526 (2009).
19. Renninger, W. H. & Chong, A. Giant-chirp oscillators for short-pulse fiber amplifiers. *Opt. Lett.* **33**, 3025 (2008).
20. Oktem, B., Ülgüdür, C. & Ilday, F. Ö. Soliton–similariton fibre laser. *Nat. Photonics* **4**, 307–311 (2010).
21. Ortaç, B. et al. Characterization of an ytterbium-doped double-clad fiber laser passively mode-locked by nonlinear polarization rotation. *Appl. Phys. B.* **77**, 589–594 (2003).
22. Bale, B. G., Kieu, K., Kutz, J. N. & Wise, F. W. Transition dynamics for multi-pulsing in mode-locked lasers. *Opt. Express* **17**, 23137–23146 (2009).
23. Kelly, S. M. Characteristic sideband instability of periodically amplified average soliton. *Electron. Lett.* **28**, 806 (1992).
24. Gordon, J. P. Dispersive perturbations of solitons of the nonlinear Schrödinger equation. *J. Opt. Soc. Am. B.* **9**, 91–97 (1992).
25. Peng, J., Boscolo, S., Zhao, Z. & Zeng, H. Breathing dissipative solitons in mode-locked fiber lasers. *Sci. Adv.* **5**, eaax1110 (2019).
26. Liu, M. et al. Visualizing the 'invisible' soliton pulsation in an ultrafast laser. *Laser Photonics Rev.* **14**, 1900317 (2020).
27. Wu, X. et al. Farey tree and devil's staircase of frequency-locked breathers in ultrafast lasers. *Nat. Commun.* **13**, 5784 (2022).
28. Wang, Z., Coillet, A., Hamdi, S., Zhang, Z. & Grelu, P. H. Spectral pulsations of dissipative solitons in ultrafast fiber lasers: period doubling and beyond. *Laser Photon. Rev.* **17**, 2200298 (2023).
29. Sugavanam, S., Kopae, M. K., Peng, J., Prilepsky, J. E. & Turitsyn, S. K. Analysis of laser radiation using the nonlinear Fourier transform. *Nat. Commun.* **10**, 5663 (2019).
30. Zhou, Y. et al. Unveiling laser radiation of multiple optical solitons by nonlinear Fourier transform. *Laser Photon. Rev.* **17**, 2200731 (2023).
31. Chang, W., Ankiewicz, A., Soto-Crespo, J. M. & Akhmediev, N. Dissipative soliton resonances. *Phys. Rev. A.* **78**, 023830 (2008).
32. Grelu, P., Chang, W., Ankiewicz, A., Soto-Crespo, J. M. & Akhmediev, N. Dissipative soliton resonance as a guideline for high-energy pulse laser oscillators. *J. Opt. Soc. Am. B.* **27**, 2336 (2010).
33. Stepien, W. & Marciante, J. R. Review of ultrafast fiber oscillators based on Mamyshev and dissipative soliton resonance mechanisms. *J. Opt. Soc. Am. B.* **39**, 626 (2022).
34. Ortaç, B., Baumgartl, M., Limpert, J. & Tunnermann, A. Approaching microjoule-level pulse energy with mode-locked femtosecond fiber lasers. *Opt. Lett.* **34**, 1585 (2009).
35. Edelmann, M. et al. Large-mode-area soliton fiber oscillator mode-locked using NPE in an all-PM self-stabilized interferometer. *Appl. Opt.* **62**, 1672 (2023).
36. Wright, L. G., Christodoulides, D. N. & Wise, F. W. Spatiotemporal mode-locking in multimode fiber lasers. *Science* **358**, 94 (2017).

37. Cao, B. et al. Spatiotemporal mode-locking and dissipative solitons in multimode fiber lasers. *Light. Sci. Appl.* **12**, 260 (2023).
38. Krupa, K. et al. Spatial beam self-cleaning in multimode fibres. *Nat. Photon.* **11**, 237 (2017).

Acknowledgements

Author contributions

M.M. performed the experimental studies and numerical simulations with support from A.C. and P.G. All authors contributed to the write-up of the manuscript. P.G. and A.C. supervised the work.

Competing interests

The authors declare the following competing interest: the authors have filed the patent application EP24305371.7, which discloses parts of this work, through the French SATT (Société d'Accélération de Transfert de Technologie) SAYENS.

Additional information

Supplementary information The online version contains supplementary material available at https://doi.org/10.1038/s41467-024-52954-7.

Correspondence and requests for materials should be addressed to Mostafa I. Mohamed or Philippe Grelu.

Peer review information *Nature Communications* thanks the anonymous, reviewer(s) for their contribution to the peer review of this work. A peer review file is available.

Reprints and permissions information is available at http://www.nature.com/reprints

Publisher's note Springer Nature remains neutral with regard to jurisdictional claims in published maps and institutional affiliations.